Interleukin-1β promotes atheroprotective changes of advanced atherosclerotic lesions in mice

Delphine Gomez[1,2,3,4], **Richard A. Baylis**[1,5], **Brittany G. Durgin**[1,2], **Alexandra A. C. Newman**[1,5], **Gabriel F. Alencar**[1,5], **Sidney Mahan**[3], **Cynthia St. Hilaire**[3,4], **Werner Muller**[6], **Ari Waisman**[7], **Sheila E. Francis**[8], **Emmanuel Pinteaux**[6], **Gwendalyn J. Randolph**[9], **Hermann Gram**[10], and **Gary K. Owens**[1,2,*]

[1]Robert M. Berne Cardiovascular Research Center, University of Virginia, Charlottesville, VA, USA [2]Department of Molecular Physiology and Biological Physics, University of Virginia, Charlottesville, VA, USA [3]Pittsburgh Heart, Lung, Blood and Vascular Medicine Institute, University of Pittsburgh; Pittsburgh, PA, USA [4]Division of Cardiology, University of Pittsburgh School of Medicine; Pittsburgh, PA, USA [5]Department of Biochemistry and Molecular Genetics, University of Virginia, Charlottesville, VA, USA [6]Faculty of Biology, Medicine and Health, University of Manchester, Manchester, UK [7]Institute for Molecular Medicine, University Medical Center of the Johannes Gutenberg University of Mainz, Mainz, Germany [8]Department of Infection, Immunity and Cardiovascular Disease, University of Sheffield, Sheffield, UK [9]Department of Pathology and Immunology, Washington University School of Medicine, St. Louis, MO 02114, USA [10]Novartis Institutes for Biomedical Research, Basel, Switzerland

Abstract

Despite decades of research, our understanding of the processes controlling late-stage atherosclerotic plaque stability remains poor. Although a prevailing hypothesis is that reducing inflammation may improve advanced plaque stability, direct evidence of this is lacking. Therefore, we performed intervention studies on smooth muscle cell (SMC) lineage tracing *Apoe*^{−/−} mice with advanced atherosclerosis using anti-IL-1β or IgG control antibodies. Surprisingly, we found that IL-1β antibody treatment between 18 and 26 weeks of Western diet feeding induced a marked reduction in SMC and collagen content, but increased macrophage number in the fibrous cap. There was also no change in lesion size and complete inhibition of beneficial outward remodeling.

*To whom correspondence should be addressed: Dr. Gary K. Owens, PhD, University of Virginia School of Medicine, 415 Lane Road, P.O. Box 801394, Room 1322 Medical Research Building 5, Charlottesville, VA 22908, phone: 434-924-2652, fax: 434-982-0055, gko@virginia.edu.

We also found that SMC-specific *Il1r1* KO resulted in smaller lesions nearly devoid of SMC and a fibrous cap whereas macrophage-selective loss of IL-1R1 had no effect on lesion size or composition. Taken together, results show that IL-1β promotes multiple beneficial changes in late-stage murine atherosclerosis including promoting outward remodeling and formation and maintenance of a SMC/collagen-rich fibrous cap.

Introduction

Despite decades of research, little is known about the factors and mechanisms controlling the stability of late-stage atherosclerotic lesions[1]. However, human pathology studies suggest that the cellular composition of plaques – specifically of the fibrous cap, a structure that separates the thrombogenic lesion contents from the blood – is a critical predictor of plaque rupture. Plaques with a higher ratio of CD68^{+} cells relative to ACTA2^{+} cells, presumed to be macrophages (MΦ) and smooth muscle cells (SMC), respectively, are more prone to rupture[2–4]. However, the markers used for identification of the lesion cells (e.g., ACTA2 and CD68) are not specific for SMC or MΦ during atherosclerosis, which raises questions as to the origin of these of cells, and more importantly their functional roles in late-stage complications[5]. Importantly, results of recent SMC lineage tracing studies from our lab[6,7] and others[8,9] have demonstrated that SMC play a much larger role during atherosclerosis than previously appreciated. Specifically, we found that >80% of SMC-derived cells within advanced lesions lack expression of the conventional SMC marker, ACTA2, and nearly 50% express markers of alternative cell types like MΦ or mesenchymal stem cells[7,8]. Interestingly, we found that SMC can have beneficial or detrimental roles in lesion pathogenesis depending on the nature of their phenotypic transitions. For example, Klf4-dependent transitions, including formation of SMC-derived MΦ-marker^{+} foam cells[7] exacerbate lesion pathogenesis whereas Oct4-dependent transitions[6] are necessary for the formation of a SMC-rich, protective fibrous cap. Taken together, these results highlight the importance of identifying strategies that promote beneficial while preventing detrimental changes in SMC phenotype and function.

A dominant hypothesis in atherosclerosis is that excessive inflammation or failed inflammation resolution is a major contributor to plaque development and late-stage lesion destabilization[10,11]. Indeed, there is extensive evidence that inflammation promotes atherosclerosis development (reviewed in [12]) including that global knockout of *IL-1β*[13] or the gene encoding its functional receptor, IL-1 receptor type 1 (*Il1r1*)[14] reduces plaque formation, whereas knockout of the endogenous IL-1 receptor 1 antagonist gene (*IL1ra*) increases plaque development[15]. In addition, administration of the IL-1β neutralizing antibody (mouse gevokizumab) throughout Western diet (WD) feeding in *Apoe*^{−/−} mice decreased overall plaque burden[16]. These studies strongly implicate IL-1β in promoting plaque development. However, there are currently no preclinical studies showing a benefit of inhibiting IL-1β after the establishment of advanced atherosclerosis. Importantly, the recently completed CANTOS trial tested three doses (50, 150, and 300-mg) of an anti-IL-1β antibody, canakinumab, administered quarterly to a very high-risk cohort of post-MI patients with reduced LDL cholesterol but increased hsCRP levels[17,18]. Initial results of the CANTOS Trial showed no benefit in all cause or cardiovascular (CV) mortality at any of the

drug dosages, but met its primary endpoint of a reduction in a composite index of non-fatal MI, non-fatal stroke, and CVD only with the 150 mg dosage[19]. However, a subsequent CANTOS report showed a 31% reduction in CV mortality and all-cause mortality in the subset of CANTOS subjects who achieved on-treatment hsCRP levels of <2.0mg/L[20]. However, this patient cohort represents a small fraction of all patients at risk for cardiovascular disease, and there was no direct evidence that IL-1β inhibition enhanced plaque stability. As such, there is a critical need for mechanistic studies to define how inhibition of IL-1β impacts late-stage lesion pathogenesis.

Despite a clear role for IL-1 signaling in atherosclerosis development, previous studies have not clearly defined the principle cell types that respond to IL-1β in atherosclerosis. However, two bone marrow chimeric studies have suggested that IL1 primarily acts on non-hematopoietic cell types during atherosclerosis development[21,22]. Specifically, transplantation of *Il1r1*−/− bone marrow into wild-type mice had no effect on lesion formation, whereas, transplantation of wild-type bone marrow into *Il1r1*−/− mice resulted in significantly smaller lesions, suggesting that non-hematopoietic cell types mediate IL-1 signaling during atherosclerosis development. Interestingly, Sui and co-workers[9] showed that SMC-selective deletion of the IκB kinase IKK-β, which is required for activation of NFκB, attenuated lesion development, suggesting a critical role for inflammatory signaling in SMC. The latter results are also consistent with several *in vitro* studies identifying IL-1β as a potent regulator of SMC migration and proliferation[23–25]. However, the direct role of IL-1 signaling in SMC during atherosclerosis pathogenesis is unknown.

In the current study, we tested the hypothesis that IL-1β inhibition induces beneficial changes in the setting of established atherosclerosis. To this end, we treated SMC lineage-tracing *Apoe*−/− mice with a mouse anti-IL-1β antibody between 18 and 26 or 18 and 21 weeks of WD feeding. Contrary to our expectations, late-stage IL1β antibody treatment resulted in multiple detrimental changes including i) a rapid remodeling of the fibrous cap characterized by reduced collagen and SMC content but a large increase in MΦ; and ii) no decrease in lesion size but impaired beneficial outward vessel remodeling leading to reduced lumen diameter. Equally surprising, we found that MΦ-selective KO of the *Il1r1* in *Apoe*−/− mice had no discernible effect, but SMC-specific *Il1r1* KO resulted in lesions highly enriched in MΦ relative to SMC with failure to form a SMC-rich fibrous cap. As such, these studies reveal an unanticipated beneficial role for IL-1β in the formation and maintenance of a protective SMC/collagen-rich fibrous cap during late-stage atherosclerosis.

Results

IL-1β neutralization decreased systemic and local inflammation in advanced atherosclerotic lesions

Although several studies have previously demonstrated that global disruption of IL-1 signaling inhibits lesion development in *Apoe*−/− mice[13–15], they may not predict the effects of acute inhibition of IL-1β on established atherosclerotic lesions[26]. To study the impact of IL-1β inhibition on advanced lesions, we performed intervention studies in which we administered an anti-IL-1β antibody (mouse monoclonal antibody; 10mg/kg) or an isotype matched IgG control (10mg/kg) for 8 weeks to SMC lineage tracing *Apoe*−/− mice (*Apoe*−/−

Myh11 Cre ER^T2 R26R-YFP) that had been fed a WD for 18 weeks (Fig 1a; Fig S1a). Mice were fed the same WD during the atherosclerosis lesion development (8 to 26 weeks of age) and the IL-1β antibody treatment (26 to 34 weeks of age). SMC lineage tracing *Apoe*^{−/−} mice were treated with tamoxifen between 6 and 8 weeks of age, prior to initiation of WD feeding, to permanently label mature MYH11^{+} SMC and track their fate and that of their progeny during development and progression of atherosclerosis as well as during intervention with an anti-IL1β antibody. We have previously shown that these mice exhibit high efficiency (>95%) of SMC-specific labelling by YFP expression when treated with tamoxifen from 6–8 weeks of age[7,27]. Treatment with the IL-1β antibody potently reduced systemic inflammation including a 50% decrease in the plasma concentration of Serum Amyloid-A (SAA) (Fig 1b), and similar reductions in IL-1β levels in plasma and liver (Fig 1c). Notably, liver and plasma IL-1α concentrations were unchanged (Fig S1b). IL-1β neutralization did not alter body weight or plasma cholesterol and triglyceride levels (Fig S1c–e). To unbiasedly assess the effects of IL-1β neutralization in atherosclerotic lesions, we performed RNAseq analyses on BCA and aortic arch regions from SMC lineage tracing *Apoe*^{−/−} mice after 8 weeks of treatment with the IL-1β antibody or the IgG control. Analysis of transcript expression showed that IL-1β antibody treatment induced a global reduction in inflammation within lesions as illustrated by the large number of downregulated inflammatory pathways (Fig 1d; Table S1). Interestingly, there was also downregulation of cell lineage and cell cycle regulatory pathways. The most upregulated pathways in IL-1β antibody treated mice included carbohydrate and energy metabolism (Fig 1d). To determine whether the antibody had direct neutralizing properties within the lesion, we assessed the IL-1β antibody penetration into atherosclerotic lesions using Rag1 deficient mice which do not produce mature T cells and B cells[28]. The use of *Rag1*^{−/−} mice allows for rigorous detection of the mouse monoclonal IL-1β neutralizing antibody without interference of endogenous antibodies. The IL-1β antibody was detected at higher levels than the IgG control in atherosclerotic lesions from *Rag1*^{−/−} *Apoe*^{−/−} mice fed 26 weeks with WD suggesting a direct effect of the neutralizing antibody within atherosclerotic lesions (Fig S1f). Secondly, the local inhibition of the IL-1 signaling pathway was confirmed by immunostaining showing a significant decrease in phospho-IRAK and IL-6 in SMC lineage tracing *Apoe*^{−/−} mice treated with the IL-1β antibody as compared to controls (Fig 1e). Taken together, these results demonstrate that the IL-1β antibody treatment regimen was effective at inhibiting the IL-1 signaling pathway, resulting in a decrease in both systemic and local plaque inflammation.

Neutralization of IL-1β induced multiple unexpected changes in late-stage atherosclerotic lesions

Despite effective inhibition of inflammation, analysis of atherosclerotic plaque burden and BCA plaque morphometry showed multiple unexpected results believed to be detrimental for plaque pathogenesis. IL-1β neutralization had no impact on aortic plaque burden (Fig 2a,b) or BCA lesion size (Fig 2c,d; Fig S2), but completely inhibited the beneficial outward vessel remodeling that normally occurs during plaque expansion (Fig 2c,d; Fig S2). Consequently, IL-1β antibody treated mice had significantly reduced lumen area (Fig 2d). Even more surprising, IL-1β antibody treatment resulted in a profound reduction in YFP[+] SMC and increase in YFP[−]LGALS3^{+} MΦ within the fibrous cap area (Fig 2e; Fig S3). This

change in cell composition was particularly evident in the fibrous cap area (defined as the 30μm-thick subluminal area within the lesion which is typically enriched in YFP[+] and ACTA2^{+} cells as previously reported[7]) (Fig 2f,g; Fig S3b,c). The increase in the LGALS3^{+} population within the fibrous cap area was driven by an increase in the number of non-SMC derived YFP[−]LGALS3^{+} MΦ (i.e., bone marrow-derived or resident MΦ) whereas the number of SMC-derived MΦ-like cells (i.e., YFP[+]LGALS3^{+}) was unchanged (Fig 2g). However, the proportion of YFP[+]LGALS3^{+} cells normalized to the total YFP[+] SMC population was significantly increased with IL-1β antibody treatment (Fig 2h), suggesting that YFP[+]LGALS3^{+} cells – in contrast to YFP[+] and YFP[+]ACTA2^{+} populations – might be resistant to loss or clearance following IL-1β neutralization.

The reduction in SMC content was associated with an overall decrease in the ACTA2^{+} fibrous cap thickness (Fig 2i). Moreover, inhibition of IL-1β also induced a significant reduction in collagen content within the fibrous cap area, a key index of plaque stability (Fig S4b,c). This reduction of collagen content within the fibrous cap area could be a direct consequence of the loss of SMC, described in previous studies as a major producer of collagen within the lesion [29], but could also be due to IL-1β-induced upregulation of collagenases. There was no difference in the expression of MMP3 and MMP9 (Fig S4d,e), two collagenases known to be regulated by IL-1β [30]. However, further studies of collagenase activity would be required to ascertain the mechanisms by which inhibition of IL-1β leads to collagen loss (i.e., decrease in production and/or increase in degradation). Interestingly, these changes to the fibrous cap area occurred despite having no effect on necrotic core area or intraplaque hemorrhage (Fig S4f–h), suggesting that there has not been effective lesion regression or complete resolution of lesion inflammation. Moreover, there was no difference in the lesion calcification (Fig S5a,b) nor in the proportion of YFP[+] SMC expressing RUNX2, a master regulator of SMC osteogenic transitions (Fig S5c,d).

The main features of the IL-1β inhibition described above were also observed when mice were treated with a lower dose of the IL-1β neutralizing antibody (1mg/kg) for 8 weeks (Fig S6a). Treatment with the IL-1β antibody at 1mg/kg induced a significant impairment of beneficial outward remodeling (Fig S6b,c) and reduced YFP[+] SMC and increased LGALS3^{+} MΦ within the fibrous cap (Fig S6d,e). Taken together the preceding results unexpectedly show that IL-1β is critical for maintaining a SMC/collagen-rich, MΦ-poor fibrous cap area.

Macrophage accumulation was driven by local proliferation rather than increased monocyte recruitment

To better understand the mechanisms responsible for the enrichment of MΦ and loss of SMC following 8 weeks of IL-1β inhibition, we investigated effects of 3 weeks of treatment. *Apoe*^{−/−} *Myh11* Cre ER[T2] R26R-YFP mice were treated with the IL-1β antibody (10 mg/kg) or the IgG control between 18 and 21 weeks of WD feeding (Fig 3a). Remarkably, just 3 weeks of IL-1β antibody treatment resulted in profound changes to the cellular composition of the fibrous cap characterized by an increase in the proportion of LGALS3^{+} cells and reduction in YFP[+] SMC (Fig 3b,c). This shift reflected a net increase in the number of LGALS3^{+} cells within the fibrous cap of mice treated with the IL-1β antibody (Fig 3d). The LGALS3^{+} population was composed predominantly of YFP[−]LGALS3^{+} cells,

whereas the SMC-derived YFP$^+$LGALS3$^+$ population was unchanged (Fig 3e). Furthermore, the increase in MΦ occurred predominantly in the fibrous cap area (Fig 3b). These data not only support a critical role for IL-1β in maintaining the integrity of the fibrous cap but also reveal that the fibrous cap area, as a structure, is much more plastic than previously appreciated.

To determine if the increase in LGALS3$^+$ population was driven by increased bone marrow-derived monocyte recruitment into the plaque, we quantified monocyte influx using a fluorescent latex bead trafficking assay [31,32]. In brief, Cy3-labeled beads were injected intravenously into *Apoe$^{-/-}$ Myh11* Cre ER^{T2} R26R-YFP mice one week prior to initiation of antibody treatment (Fig 4a, Fig S7a). Mice injected with beads received either the IL-1β neutralizing antibody or IgG control antibody for 3 weeks. Flow cytometry analysis of blood collected 24 hours after the bead injection demonstrated efficient labeling of circulating monocytes consistent with previous reports (Fig S7b,c)[31–33]. Importantly, there were no changes in blood cell populations after the bead and antibody treatment (Fig S7d). BCA plaques from IL-1β antibody and IgG control treated mice showed no differences in bead accumulation (Fig 4b,c). However, IL-1β antibody treated mice exhibited a marked decrease in the ratio of beads to MΦ (Fig 4c), suggesting that the MΦ accumulation induced by IL-1β inhibition was not due to an increase in newly recruited monocytes.

To determine if the accumulation of MΦ was driven by proliferation, we performed immunostaining for Ki67 on mice treated with 3 weeks of IL-1β antibody or IgG control (Fig 4d). Although the overall fraction of proliferating cells was not significantly changed (Fig 4e), treatment with the IL-1β antibody profoundly changed which cell types underwent proliferation in the fibrous cap. Specifically, there was marked reduction in YFP$^+$ SMC proliferation and an increase in MΦ (YFP$^-$LGALS3$^+$) proliferation (Fig 4e,f). However, there was no change in the proliferation of YFP$^+$LGALS3$^+$ cells indicating that the exacerbation of LGALS3$^+$ proliferation did not include SMC-derived MΦ-like cells (Fig 4f). Of note, IL-1β inhibition did not induce changes in endothelial cell proliferation (Fig S8). We also assessed the proportion of YFP+ and LGALS3+ cells undergoing apoptosis in these same samples. TUNEL (Fig 4g,h) and cleaved Caspase3 (Fig S9) analyses showed no differences in apoptosis of SMC or MΦ in IL-1β antibody treated mice as compared to controls. Taken together, these data show that inhibition of IL-1β profoundly impacts the cell composition within advanced atherosclerotic plaques primarily by inhibiting SMC proliferation and promoting proliferation of MΦ within lesions.

IL-1 signaling is required for SMC investment into lesions and the fibrous cap

The preceding observations demonstrate that inhibition of IL-1β in mice with advanced lesions resulted in a dramatic reduction in SMC and increase in MΦ within the fibrous cap. However, it is unclear if these changes were mediated via direct loss of IL-1 signaling in SMC, MΦ, or other cell types within the lesions.

Thus, to ascertain the role of IL-1 signaling in SMC on atherosclerosis development, we generated mice with tamoxifen-inducible SMC-specific *Il1r1* KO and simultaneous SMC lineage tracing by crossing *Il1r1$^{fl/fl}$* mice [34] with *Apoe$^{-/-}$ Myh11* Cre ER^{T2} R26R-YFP mice (Fig S10a). The resulting *Apoe$^{-/-}$ Myh11* Cre ER^{T2} R26R-YFP *Il1r1$^{fl/fl}$* and littermate

control $Il1r1^{WT/WT}$ mice were treated with a series of tamoxifen injections from 6 to 8 weeks of age to induce simultaneous expression of a YFP lineage tracing gene, and excision of exon 5 of the $Il1r1$ gene exclusively in SMC [7,27] (designated below as $Il1r1^{SMC\ /}$ or $Il1r1^{SMC\ WT/WT}$) before being fed a WD for 18 weeks (Fig S10b). We observed high efficiency recombination of $Il1r1$ in SMC rich tissues including aorta, carotid, and lung in tamoxifen-treated $Il1r1^{SMC\ fl/fl}$ mice (Fig S10c). Recombination of the $Il1r1$ locus was associated with corresponding reductions in IL-1R1 protein expression based on immunohistochemical staining of carotid medial SMC in $Il1r1^{SMC\ /}$ mice with an anti-IL-1R1 antibody (Fig S10d). There were no significant differences in body weight or serum cholesterol and triglyceride levels (Fig S10e–f). However, remarkably, we observed a >60% reduction in BCA plaque size in $Il1r1^{SMC\ /}$ mice as compared to $Il1r1^{SMC\ WT/WT}$ mice (Fig 5a,b), as well as a marked reduction in collagen content (Fig 5c,d) but no difference in intraplaque hemorrhage (Fig 5e,f). Of major interest, the lesions in the $Il1r1^{SMC\ /}$ mice were almost entirely devoid of SMC (YFP+) and ACTA2+ cells, but significantly enriched in YFP− LGALS3+ cells (Fig 5g–i). This was particularly evident in the fibrous cap area which exhibited an >80% reduction in YFP+ area and a 70% decrease in ACTA2+ area. In addition, fibrous cap areas from $Il1r1^{SMC\ /}$ mice had a 2.8 fold increase in LGALS3+ area (Fig 5i).

We also tested the effect of MΦ-selective $Il1r1^{-/-}$ on atherosclerosis development using $Apoe^{-/-}$ $LysM$ Cre R26R-YFP $Il1r1^{fl/fl}$ and $Apoe^{-/-}$ $LysM$ Cre R26R-YFP $Il1r1^{WT/WT}$ littermate control mice fed WD for 18 weeks (Fig S11a,b). Importantly, this $LysM$ Cre gene targeting results in efficient gene targeting of monocytes, mature macrophages and granulocytes [35]. LysM cre driven knockout of IL1R1 induced a complete inhibition of the IL-1 signaling pathway as demonstrated by the lack of IRAK phosphorylation in LGALS3+YFP+ cells within atherosclerotic lesions of $Il1r1^{MΦ\ /}$ (Fig S11e). In contrast to the profound effects of SMC-specific $Il1r1$ deletion, there was no significant effect of losing IL-1R1 in LysM expressing cells on vessel size, lesion size, or the frequency of YFP+, LGALS3+, or ACTA2+ cells (Fig S12). Taken together, these cell-specific $Il1r1$ KO studies provide compelling evidence that IL-1 signaling in SMC, rather than myeloid cells, plays a critical role during atherosclerosis development. Moreover, results suggest that the reductions in indices of plaque stability observed in our IL-1β neutralization experiments, including the marked loss of SMC and collagen, as well as increases in MΦ within the fibrous cap, are due, at least in part, to disrupted IL-1 signaling in SMC.

IL-1β neutralization increased IL-4 levels and promoted macrophage M2 polarization

To determine potential mechanisms altering the cellular composition of the fibrous cap following IL-1β antibody treatment, we performed a cytokine and chemokine array on BCA tissue extracts from mice treated with 8 weeks of either IL-1β or control antibody (Fig 6a). Interestingly, there was a two-fold increase in IL-4 protein in BCA lesions from the IL-1β antibody treated mice. Of interest, IL-4 has been shown to inhibit SMC [36,37] but promote resident MΦ proliferation [38,39], consistent with our *in vivo* KI67 staining data (Fig 4). IL-4 has also been identified as a key cytokine involved in M2 polarization of MΦ *in vitro* [40,41]. To better understand the impact of IL-1β neutralization on macrophage phenotype, we performed staining for classic M1 (iNOS) and M2 (Arg1) markers. Although there are considerable limitations to the M1/M2 paradigm, confocal analyses of these markers permits

studies of individual MΦs within the fibrous cap and their possible functions. Consistent with increased IL-4, there was a decrease in the number of LGALS3^{+}iNOS[+], but a large increase in Arg1^{+} expressing macrophages within the fibrous cap area (Fig 6b,c). These results suggest that IL-1β neutralization induces an anti-inflammatory phenotype in resident MΦ within the fibrous cap that is mediated, at least in part, by increased IL-4.

Discussion

Our present study provides compelling evidence of a critical role for IL-1 signaling during late-stage atherosclerosis. However, contrary to our expectations, IL-1 signaling appeared to play multiple beneficial roles that were lost by either IL-1β neutralization or SMC-specific knockout of *Il1r1*. Indeed, although lesions from SMC-specific *Il1r1* KO *Apoe*^{−/−} mice were smaller, they exhibited a number of changes believed to be detrimental including failure to form a protective ACTA2^{+} fibrous cap, reduced in collagen content, and increased in MΦ content. Likewise, IL-1β antibody treatment of SMC lineage tracing *Apoe*^{−/−} mice with advanced atherosclerosis decreased multiple plaque stability indices including a 40% decrease in SMC content, >50% decrease in ACTA2^{+} coverage, 30% reduction in collagen content, and 50% increase in MΦ (M2) content within the fibrous cap. Taken together, these observations have several important implications. **First,** our results indicate an unexpected role for IL-1β in regulating fibrous cap formation in advanced lesions and suggest that excessive inhibition of inflammation could have detrimental effects. Tabas and co-workers have long emphasized the importance of improving inflammation resolution, rather than suppression, as a key therapeutic approach for stabilizing lesions [10,42,43]. **Second,** the fibrous cap is far more plastic than anticipated, a finding that if true in humans, may have important implications for atherosclerotic disease management and development of more effective therapeutic approaches. **Third,** our results highlight the need for increased emphasis on intervention rather than prevention models in preclinical atherosclerosis studies seeking to identify novel therapies for treating advanced atherosclerosis [26]. The importance of this concept is made This concept is particularly clear when comparing the previous prevention study that treated *Apoe*^{−/−} mice from the beginning of WD feeding with an IL-1β antibody and showed reduced plaque formation[16], with our intervention study that showed no improvement on the same measurement and changes consistent with plaque destabilization. Therefore, one cannot assume that pharmacologic agents that are effective at preventing fatty streak formation in young animals will necessarily have beneficial effects in the setting of established atherosclerosis.

One of the most striking observations following IL-1β neutralization in advanced lesions was the loss of SMC but increase in MΦ within the fibrous cap. Our data suggest this is driven in part by reduced SMC proliferation, which is consistent with *in vitro* studies that IL-1β induces SMC proliferation [24,25]. However, it is also possible that global IL-1β inhibition may be associated with impaired migration and/or homing of SMC and/or MΦ into the fibrous cap due to changes in the production or sensitivity to guidance cues. Consistent with this possibility, Moore and co-workers [44,45] have identified several MΦ chemo-attractant and chemo-repulsive proteins whose production by SMC could be regulated by IL-1β. However, the accumulation of MΦ was driven by local proliferation of MΦ rather than increased monocyte recruitment from the blood. These observations are

consistent with studies by Swirski and co-workers [46] showing that local proliferation of MΦ, rather than monocyte trafficking, regulates MΦ expansion in established lesions.

Of interest, we present correlative evidence suggesting that increased expression of IL-4 may contribute to reduced proliferation of SMC while simultaneously stimulating proliferation of local MΦ and their M2 polarization. Consistent with this possibility, IL-4 has previously been shown to induce these changes in cultured SMC and macrophages respectively [36,38,39]. Although M2 MΦ have been shown to play a beneficial role in atherosclerosis pathogenesis, it remains to be determined whether an influx of M2 or M2-like MΦ into the fibrous cap would be beneficial or detrimental. However, our results suggest that this may be detrimental due to: 1) the loss of SMC and collagen; and 2) the increase in M2 MΦ occurred despite failure to resolve the necrotic core, reduce the extent of intraplaque hemorrhage or calcification, or clear plaque cholesterol crystals[47]. That is, global IL-1β suppression may be inducing a false-sense of inflammation resolution that results in premature dissolution of the SMC/collagen-rich fibrous cap. Consistent with this possibility, our SMC *Il1r1* knockout studies indicate that IL-1 signaling is required for investment of these cells into the fibrous cap (Figure 5). In addition, IL-1β potently induces multiple processes in cultured SMC that are likely to be important in fibrous cap formation and maintenance including proliferation [24], migration [30], and collagen synthesis [29].

A critical question is to determine to what extent, if any, our IL-1β antibody intervention studies in mice translate to patients, including those in the CANTOS Trial [19]. The results of CANTOS represent a major advance for the cardiovascular field for several reasons. First, they [19,20] provide the most direct evidence to date validating the inflammation hypothesis of atherosclerosis in man. Second, they are the first to achieve a reduction in CV risk in high risk subjects with advanced atherosclerotic disease via a therapy independent of lipid lowering (see our editorial[48] and others[49,50]). However, it is critical to appreciate that: 1) CANTOS met its primary endpoint only at the intermediate of three doses tested; and 2) an overall benefit on all cause and cardiovascular mortality was restricted the subset of CANTOS subjects who achieved on-treatment hsCRP levels of <2.0mg/L [20]. These latter results are quite exciting in that they indicate that canakinumab may be an appropriate therapy for this subset of very high risk post-MI patients, but would seem to be at odds with our findings that IL-1β antibody treatment of *Apoe*$^{-/-}$ mice with advanced lesions resulted in rapid loss of SMC and collagen within the fibrous cap (Figures 2–3).

However, there are major limitations in directly comparing our mouse intervention studies with the outcome of the CANTOS Trial. **First**, there are inherent differences between humans and mice including differences in disease time-course and treatment periods, as well as fundamental immune system differences, and lack of genetic diversity in mice. In addition, >80% of CANTOS subjects had a percutaneous coronary intervention or coronary bypass; >90% were taking antithrombotic, lipid-lowering, and/or anti-ischemic agents; and >79% were on inhibitors of the renin-angiotensin system. **Second**, it is possible that we are modeling fundamentally different mechanisms than those operative in CANTOS patients including effects of a prior MI and associated infarct remodeling that was not a component of our experimental design. **Third**, there are several studies reporting improved glycemic control and insulin sensitivity with inhibition of IL-1 signaling[9,51,52]. However, a recent

report showed that, within the CANTOS trial patient cohort, canakinumab had similar effects on occurrence of CV events among patients with diabetes or pre-diabetes but the treatment itself did not reduce diabetes incidence[53]. **Fourth**, our mice are severely hypercholesterolemic whereas the CANTOS patients had relatively well managed cholesterol levels (e.g., LDL cholesterol <83mg/dL). We feel this may be an absolutely critical determinant of the effects of global IL-1β suppression in the context of advanced atherosclerosis. Indeed, in light of the marked increase in cardiovascular deaths resulting from widespread use of the anti-inflammatory COX2 inhibitor rofecoxib (Vioxx)[54], a major challenge moving forward will be to determine to what extent canakinumab or other broadly acting anti-inflammatory agents should be extended to lower-risk patients. Specifically, it will be critical to determine strategies to identify subsets of patients that will exhibit the most benefit from these therapies, and perhaps more importantly to determine if there are patients that may be more susceptible to the adverse effects. In support of this hypothesis, two clinical studies are consistent with our findings and suggest that inhibition of IL-1 signaling may unexpectedly increase the risk of some cardiovascular events. **First**, the MRC-ILA Heart Study was a Phase IIb, double-blinded, randomized, placebo-controlled study of Anakinra, a recombinant IL-1 receptor antagonist (IL-1ra), administered for two weeks to patients following a non-ST elevation MI [55]. Although not powered to measure long-term outcomes, the study showed that Anakinra treatment increased major adverse cardiovascular events, including MI, at one year by greater than four-fold. **Second**, studies by the IL-1 Genetics Consortium [56] investigated two common variants located upstream of the *IL-1ra* locus known to increase its expression. This retrospective study of 746,171 patients showed that increased levels of IL-1ra are correlated with reduced hs-CRP and IL-6, consistent with reduced systemic inflammation, but with an allele-dependent increase in coronary artery disease. As such, we believe the greatest value of our late-stage atherosclerosis intervention studies in mice is to generate hypotheses, which might then be tested in man to better understand the mechanistic and physiological aspects of IL-1β inhibition. In addition, armed with a greater understanding of the basic vascular biology, the field can identify alternative (or combinatorial) anti-inflammatory therapeutic targets that are both effective and safe for treating a broader and lower risk cohort of human subjects.

Online Methods

Study Design

The objectives of these studies were to determine the effects of IL-1β inhibition on established atherosclerotic lesions and to identify the consequences of IL-1β neutralization and cell-specific loss of IL-1 signaling. To achieve this, we performed an intervention study in which atheroprone *Apoe*$^{-/-}$ were treated with a mouse monoclonal anti-IL-1β antibody provided by Novartis following 18 weeks of Western Diet (WD). At this time point, brachiocephalic arteries consistently develop advanced atherosclerotic lesions with common features of end-stage human lesions including large necrotic cores, collagen-rich fibrous caps, and intraplaque hemorrhage. The dose of the antibody and the duration of the treatment were prospectively selected based on the pharmacokinetic properties of the antibody. We utilized the well-characterized SMC lineage tracing *Apoe*$^{-/-}$ *Myh11* Cre ER^{T2} R26R YFP [7,27,57] mice to rigorously lineage trace SMC and perform qualitative and

quantitative assessment of their presence, location, and phenotypic characteristics. $Apoe^{-/-}$ $Myh11$ Cre ER^{T2} R26R YFP mice were crossed to $Il1r1$ floxed mice (fl/fl) to generate tamoxifen-inducible SMC-specific lineage tracing and $Il1r1$ KO mice. We utilized $Il1r1^{wt/wt}$ and $Il1r1^{fl/fl}$ littermates to ensure that the IL-1R1 deficient and control animals were genetically identical with exception to the $Il1r1$ locus. All mice were on a C57Bl/6 background and had been backcrossed at least 8 generations. Although it would be ideal to study IL-1β neutralization in both males and females, the $Myh11$ Cre ER^{T2} transgene is located on the Y chromosome preventing us from using females in this study. A power analysis with 95% power and α=0.05 indicated that a sample size of at least 6 mice per group was required for morphometry and immunofluorescence analysis and a minimum of 3 mice per group for the bead assay. We routinely exceeded the minimal number of mice required for each experiment as indicated in the figure legends. All data were included and outliers, if any, were not excluded. Only mice with a plasma cholesterol level <500 g/dL and thus not considered hypercholesterolemic were excluded from analyses.

Animals, diet and treatment

Animal protocols were approved by the University of Virginia Animal Care and Use Committee. The $Apoe^{-/-}$ $Myh11$ Cre ER^{T2} R26R-YFP mice used in the intervention study have been described in previous studies [6,7,27]. These mice were crossed with $Il1r1^{fl/fl}$ mice that were generated, characterized [34], and provided by Dr. Emmanuel Pinteaux. Male $Apoe^{-/-}$ $Myh11$ Cre ER^{T2} $Il1r1^{fl/wt}$ R26R-YFP and $Apoe^{-/-}$ $Il1r1^{fl/wt}$ R26R-YFP female mice were bred to generate $Apoe^{-/-}$ $Myh11$Cre ER^{T2} $Il1r1^{fl/fl}$ or $^{wt/wt}$ R26R-YFP littermate experimental mice. Male $Apoe^{-/-}$ $LysM$ Cre $Il1r1^{fl/fl}$ or $^{wt/wt}$ R26R-YFP littermates were generated in a similar fashion. All mice were carefully genotyped by PCR as previously described [27,34,57]. In $Myh11$ Cre ER^{T2} mice, Cre recombinase was activated with a series of ten tamoxifen injections (1mg/day/mouse; Sigma Aldrich, T-5648) over a 2-week period. One week after the tamoxifen treatment, mice were fed a high fat Western-type diet (WD), containing 21% milk fat and 0.15% cholesterol (Harlan Teklad; TD.88137) for either 18, 21 or 26 weeks. Prior to beginning WD, mice were fed a standard chow diet purchased from Harlan Teklad (TD.7012). For our intervention studies, $Apoe^{-/-}$ $Myh11$ Cre ER^{T2} R26R-YFP mice received intraperitoneal (I.P.) injections of anti-IL-1β antibody or IgG control (provided by Novartis) when they reached 18 weeks of WD feeding for either 3 or 8 weeks while remaining on WD. Anti-IL-1β antibody or IgG control were injected weekly at the concentrations 10 mg/kg or 1 mg/kg. To ensure advanced lesions, the $Rag1^{-/-}Apoe^{-/-}$ mice were fed 26 weeks of WD prior to starting a series of 8 weekly injections with the IL-1β antibody or the IgG control (10mg/kg). Mice were euthanized by CO_2 asphyxiation after overnight fasting, and peripheral blood was collected by cardiac puncture. Whole blood and plasma were used respectively for circulating blood cell count and cholesterol and triglyceride analyses, which were performed by the University of Virginia Clinical Pathology Laboratory. Immediately after CO_2 asphyxiation, mouse carcasses were perfused via the left ventricle with 5 mL PBS, 10 mL 4% paraformaldehyde, and 5 mL PBS. Brachiocephalic arteries (BCA) were then dissected, processed and embedded in paraffin.

Plaque burden analysis by Sudan IV staining

Aortas from *Apoe*^{−/−} *Myh11* Cre ER[T2] R26R-YFP mice treated with anti-IL-1β antibody or IgG control for 8 weeks were dissected from the aortic arch to the iliac bifurcation and subjected to en face Sudan IV staining (n=6 per group). In brief, after carefully removing the peri-adventitial fat, aortas were dehydrated in 70% ethanol for 5 minutes and incubated in Sudan IV solution for 6 minutes, which was prepared as follows: 1 g of Sudan IV (Sigma Aldrich, S4261) was diluted in 100 mL of 70% ethanol and 100 mL of 100% acetone. Finally, aortas were differentiated in 80% ethanol for 3 minutes and stored in PBS at 4°C.

Immunohistochemistry and atherosclerotic plaque morphometry

Paraformaldehyde-fixed paraffin-embedded BCAs were serially cut in 10 μm thick sections from the aortic arch to the bifurcation of the right subclavian artery. For morphometric analysis, we performed modified Russell-Movat staining on three locations along the BCA at 150 μm, 450 μm, and 750 μm from the aortic arch as previously described [6,7]. The lumen, lesion, and necrotic core areas as well as the external elastic lamina (vessel area), the internal elastic lamina, the medial area and the medial thickness were measured on digitized images of the Movat staining using Image Pro Plus Software 7.0 (Media Cybernetics). Picrosirius Red and Von Kossa staining were performed to assess collagen content and calcification, respectively. Immunohistochemistry (IHC) was performed with antibodies against IRAK phospho-T209 (4 μg/mL, Abcam), IL-6 (4 μg/mL, Bioss antibodies) IL1R1 (4 μg/mL, Bioss Antibodies), MMP3 (7.7 μg/mL, ab53015, Abcam), MMP9 (2 μg/mL, ab38898, Abcam) and TER-119 (1 μg/mL, Santa-Cruz Biotechnology). Staining for immunohistochemistry was visualized by DAB (Acros Organics). Integrated Optical Densitometry analysis of DAB staining was performed using Image Pro Plus Software 7.0 (Media Cybernetics).

Immunofluorescent staining

BCA sections were de-paraffinized and rehydrated in xylene and ethanol series. After antigen retrieval (H-3300, Vector Laboratories), sections were blocked with fish skin gelatin–PBS (6 g/L) containing 10% horse serum for 1 hour at room temperature. Slides were incubated with the following antibodies: mouse monoclonal SM α-actin-FITC (ACTA2) (4.4 μg/mL, clone 1A4, Sigma Aldrich), goat polyclonal anti-GFP (4 μg/mL, ab6673, Abcam) for detection of YFP, LGALS3 (2 μg/mL, Cedarlane CL8942AP), RUNX2 (1.374 μg/mL, ab192256, Abcam), Ki67 (4 μg/mL, ab15580, Abcam), PECAM-1 (1 μg/mL, Santa Cruz), IRAK phosphor-T209 (4 μg/mL, Abcam), iNOS (0.52 μg/mL, ab15323, Abcam), and Arg1 (9.2 μg/mL, GTX109242, GeneTex). The secondary antibodies were donkey anti-rat conjugated to Alexa 555 (5 μg/mL, Abcam), donkey anti-rat conjugated to Alexa 647 (5 μg/mL, Abcam), donkey anti-goat conjugated to Alexa 555 (5 μg/mL, Invitrogen), and donkey anti-goat conjugated to Alexa 647 (4 μg/mL, Invitrogen). Apoptosis was assessed by TUNEL (CF488A, Biotium) and cleaved caspase 3 staining (0.84 ug/mL, ab9661, Cell Signaling Technology). IL-1β antibody was detected using a donkey anti-mouse IgG2a-Alexa 488 antibody. DAPI (0.05 mg/mL, D3571, ThermoFisher Scientific) was used as a nuclear counterstain and slides were mounted using Prolong Gold Antifade (Invitrogen).

Monocyte Trafficking - Bead Assays

Apoe$^{-/-}$ *Myh11* Cre ER^{T2} R26R-YFP mice fed a Western Diet (Harlan Teklad; TD.88137) for 17 weeks received an injection of Fluoresbrite Polychromic Red 1.0 micron beads (2.5% solids-latex; Polysciences, Inc., #18660). Beads were diluted in sterile PBS (1:4 dilution) and 250 µL of diluted beads were injected retro-orbitally. 24 hours after the injection, blood was collected by tail bleeding and selective uptake of the beads by circulating Ly6C^{low} monocytes was assessed by flow cytometry (see Flow cytometry section). 5–7 days after the bead injection, we started the anti-IL-1β antibody or IgG control regimen (10 mg/kg) for a duration of 3 weeks as described above. At the end of the antibody treatment, mice were euthanized by asphyxiation. Mice were perfusion fixed with Periodate-Lysine-Paraformaldehyde (PLP). Each BCA was harvested, post-fixed in PLP, and incubated in a gradient of sucrose solutions before being embedded in O.C.T. compound. Serial frozen 10 µm-thick sections were used to perform immunofluorescent staining for LGALS3 (Cedarlane CL8942AP) and DAPI for nuclear staining. Endogenous fluorescent signal of Fluoresbrite Polychromic Red beads was directly detectable.

Imaging

Movat, IL1R1, MMP3, Ter119 and Sudan IV staining of brachiocephalic arteries were imaged using a Zeiss Axioskope2 microscope equipped with an AxioCamMR3 camera. Image acquisition was performed with AxioVision40 version 4.6.3.0 software (Carl Zeiss Imaging Solution). Digitized images were analyzed with Image Pro Plus Software 7.0 (Media Cybernetics). Immunofluorescent staining was imaged using either a Zeiss LSM700 or a Nikon A1 confocal microscope to acquire a series of eight *z*-stack images at 1-µm intervals. Zen 2009 Light Edition Software (Zeiss) or NIS-Element 5.02 Software (Nikon) were used for analysis of each *z*-stack image and single-cell counting was performed for phenotyping and quantifying the cell population comprised within the 30µm thick layer proximal to the lumen (i.e., fibrous cap area). Assessment of YFP$^+$, ACTA2$^+$, and LGALS3$^+$ areas (normalized to lesion or fibrous cap area) was performed using maximal intensity projection images and the analysis was done using Image Pro Plus Software 7.0 (Media Cybernetics). Maximal intensity projection of representative images were used to generate the representative images included in the figures and Adobe Photoshop was used to process and format images.

RNA-seq and Data Analysis

RNA sequencing and analysis—Total RNA was isolated using Trizol (Invitrogen) from the BCA and aortic arch region of *Apoe*$^{-/-}$ *Myh11* Cre ER^{T2} R26R-YFP mice fed a high-fat Western diet for 26 weeks and treated with the anti-IL1β antibody ($n = 4$) or with the IgG control antibody ($n = 4$) for the last 8 weeks of high-fat Western diet feeding (18 to 26 weeks). The RNA library was prepared according to Illumina RNA Seq library kit instructions with rRNA reduction and the deep sequencing was performed by the HudsonAlpha Institute for Biotechnology. Quality control and quantification of RNA and library were performed using an Agilent 2100 Bioanalyzer and a Kapa Library Quantification Kit (Kapa Biosystems), according to the manufacturer's protocol. Libraries were sequenced with the Illumina HiSeq2000 (2×100 bp).

Sequence analysis of RNA reads—100 nt paired-end reads were mapped to the mm9 reference genome using STAR software version 2.4 [58]. A table of gene counts/quantification was generated using FeatureCounts in the Subread package [59]. We used the DESeq2 Bioconductor R package [60] to identify differentially expressed genes at a 5% false discovery rate (FDR) (P_{adj} 0.05) using the Benjamini–Hochberg procedure to adjust P values. GENCODE/Ensembl gene IDs mapping to known genes were used, whereas those mapping to predicted genes were excluded. Gene set enrichment analysis (GSEA) was performed using GAGE [61]. GSEA included cutoff free gene expression data. Significantly enriched pathways were identified using a 5% FDR cutoff, and their enrichment significance was quantified using $-\log_{10}$ of P_{adj}. A functional annotation analysis of the differentially enriched pathway was performed using PANTHER and Gene Ontology Consortium (http://geneontology.org/) software. Data are presented as pathways downregulated or upregulated in IL-1β antibody treated mice as compared to IgG control treated mice. The RNA-seq data is available at the NCBI Gene Ontology Omnibus (GEO) database under GEO accession number GSE111535.

Flow Cytometry

Blood samples were acquired by either tail bleed or terminal cardiac puncture. Red blood cells and platelets were cleared using in RBC lysis buffer (BD PharmLyse 555899) and Hanks Balanced Salt Solution (Gibco 14185). Dead cells were eliminated using Live-Dead Fixable Yellow (0.55 μL/mL; Thermo-Fisher L34959). Prior to surface staining, Fc receptors were blocked with TruStain fcX anti-mouse CD16/32 antibody (10 μg/mL; Biolegend; 101320). Cells were stained with the following antibodies CD45 (5 μg/mL; eBiosciences; clone: 30-F11), CD11b (2.5 μg/mL; eBiosciences; clone: M1/70), Ly6C (2.5 μg/mL; Biolegend, clone: HK1.4), Ly6G (2.5 μg/uL; Biolegend; clone: 1A8), and CD115 (0.6 μg/mL; eBiosciences; clone: AFS98). OneComp ebeads (50 μL/sample; eBiosciences; 01-1111-42) were used for single stain controls and all experiments used fluorescent minus one (FMO) controls for each marker. All samples were run on a Beckman Coulter CyAn ADP LX flow cytometer equipped with 405-nm, 488-nm, and 633-nm lasers and analyzed using FlowJo Version 10 software.

Statistical analysis

Statistics were performed using GraphPad Prism 6. Data normality was determined using the Kolmogorov-Smirnov test. For comparison of two groups of continuous variables with normal distribution and equal variances, two-tailed unpaired Student's *t*-tests were performed with a confidence level of 95%. For comparison of two groups of continuous variables with normal distribution and unequal variances, two-tailed unpaired Student's *t*-tests followed by a Welch's correction were performed with a confidence level of 95%. Two-tailed unpaired Mann-Whitney *U*-tests with a confidence level of 95% were conducted if data were non-normally distributed. For multiple group comparison, we performed two-tailed one-way or two-ways ANOVA. For categorical data (calcification and intraplaque hemorrhage analysis), we used a Fisher's exact test. All data were included and outliers, if any, were not excluded. Only mice with a plasma cholesterol level <500 g/dL and thus not considered hypercholesterolemic were excluded from analyses. The number of mice used for each analysis is indicated in the figure legends. Statistical significance threshold was set at

P $\leq$ 0.05. The exact P value is indicated for each statistical test. All data are presented as the mean ± SEM.

See our Life Sciences Reporting Summary available online for additional information about experimental design and reagents.

Supplementary Material

Refer to Web version on PubMed Central for supplementary material.

Acknowledgments

References

1. Yahagi K, et al. Pathophysiology of native coronary, vein graft, and instent atherosclerosis. Nat Rev Cardiol. 2016; 13:79–98. DOI: 10.1038/nrcardio.2015.164 [PubMed: 26503410]

2. Kolodgie FD, et al. Pathologic assessment of the vulnerable human coronary plaque. Heart. 2004; 90:1385–1391. DOI: 10.1136/hrt.2004.041798 [PubMed: 15547008]

3. Virmani R, Kolodgie FD, Burke AP, Farb A, Schwartz SM. Lessons from sudden coronary death: a comprehensive morphological classification scheme for atherosclerotic lesions. Arterioscler Thromb Vasc Biol. 2000; 20:1262–1275. [PubMed: 10807742]

4. Davies MJ, Richardson PD, Woolf N, Katz DR, Mann J. Risk of thrombosis in human atherosclerotic plaques: role of extracellular lipid, macrophage, and smooth muscle cell content. Br Heart J. 1993; 69:377–381. [PubMed: 8518056]

5. Gomez D, Owens GK. Smooth muscle cell phenotypic switching in atherosclerosis. Cardiovasc Res. 2012; 95:156–164. DOI: 10.1093/cvr/cvs115 [PubMed: 22406749]

6. Cherepanova OA, et al. Activation of the pluripotency factor OCT4 in smooth muscle cells is atheroprotective. Nat Med. 2016; 22:657–665. DOI: 10.1038/nm.4109 [PubMed: 27183216]

7. Shankman LS, et al. KLF4-dependent phenotypic modulation of smooth muscle cells has a key role in atherosclerotic plaque pathogenesis. Nat Med. 2015; 21:628–637. DOI: 10.1038/nm.3866 [PubMed: 25985364]

8. Feil S, et al. Transdifferentiation of vascular smooth muscle cells to macrophage-like cells during atherogenesis. Circ Res. 2014; 115:662–667. DOI: 10.1161/CIRCRESAHA.115.304634 [PubMed: 25070003]

9. Sui Y, et al. IKKbeta links vascular inflammation to obesity and atherosclerosis. J Exp Med. 2014; 211:869–886. DOI: 10.1084/jem.20131281 [PubMed: 24799533]

10. Tabas I, Glass CK. Anti-inflammatory therapy in chronic disease: challenges and opportunities. Science. 2013; 339:166–172. DOI: 10.1126/science.1230720 [PubMed: 23307734]

11. Libby P, Tabas I, Fredman G, Fisher EA. Inflammation and its resolution as determinants of acute coronary syndromes. Circ Res. 2014; 114:1867–1879. DOI: 10.1161/CIRCRESAHA.114.302699 [PubMed: 24902971]

12. Hansson GK, Libby P, Tabas I. Inflammation and plaque vulnerability. J Intern Med. 2015; 278:483–493. DOI: 10.1111/joim.12406 [PubMed: 26260307]

13. Kirii H, et al. Lack of interleukin-1beta decreases the severity of atherosclerosis in ApoE-deficient mice. Arterioscler Thromb Vasc Biol. 2003; 23:656–660. DOI: 10.1161/01.ATV. 0000064374.15232.C3 [PubMed: 12615675]

14. Chi H, Messas E, Levine RA, Graves DT, Amar S. Interleukin-1 receptor signaling mediates atherosclerosis associated with bacterial exposure and/or a high-fat diet in a murine apolipoprotein E heterozygote model: pharmacotherapeutic implications. Circulation. 2004; 110:1678–1685. DOI: 10.1161/01.CIR.0000142085.39015.31 [PubMed: 15353494]

15. Isoda K, et al. Lack of interleukin-1 receptor antagonist modulates plaque composition in apolipoprotein E-deficient mice. Arterioscler Thromb Vasc Biol. 2004; 24:1068–1073. DOI: 10.1161/01.ATV.0000127025.48140.a3 [PubMed: 15059807]

16. Bhaskar V, et al. Monoclonal antibodies targeting IL-1 beta reduce biomarkers of atherosclerosis in vitro and inhibit atherosclerotic plaque formation in Apolipoprotein E-deficient mice. Atherosclerosis. 2011; 216:313–320. DOI: 10.1016/j.atherosclerosis.2011.02.026 [PubMed: 21411094]

17. Ridker PM, et al. Effects of interleukin-1beta inhibition with canakinumab on hemoglobin A1c, lipids, C-reactive protein, interleukin-6, and fibrinogen: a phase IIb randomized, placebo-controlled trial. Circulation. 2012; 126:2739–2748. DOI: 10.1161/CIRCULATIONAHA. 112.122556 [PubMed: 23129601]

18. Ridker PM, Thuren T, Zalewski A, Libby P. Interleukin-1beta inhibition and the prevention of recurrent cardiovascular events: rationale and design of the Canakinumab Anti-inflammatory Thrombosis Outcomes Study (CANTOS). Am Heart J. 2011; 162:597–605. DOI: 10.1016/j.ahj. 2011.06.012 [PubMed: 21982649]

19. Ridker PM, et al. Antiinflammatory Therapy with Canakinumab for Atherosclerotic Disease. N Engl J Med. 2017

20. Ridker PM, et al. Relationship of C-reactive protein reduction to cardiovascular event reduction following treatment with canakinumab: a secondary analysis from the CANTOS randomised controlled trial. Lancet. 2018; 391:319–328. DOI: 10.1016/S0140-6736(17)32814-3 [PubMed: 29146124]

21. Chamberlain J, et al. Interleukin-1 regulates multiple atherogenic mechanisms in response to fat feeding. PLoS One. 2009; 4:e5073. [PubMed: 19347044]

22. Shemesh S, et al. Interleukin-1 receptor type-1 in non-hematopoietic cells is the target for the pro-atherogenic effects of interleukin-1 in apoE-deficient mice. Atherosclerosis. 2012; 222:329–336. DOI: 10.1016/j.atherosclerosis.2011.12.010 [PubMed: 22236482]

23. Alexander MR, Murgai M, Moehle CW, Owens GK. Interleukin-1beta modulates smooth muscle cell phenotype to a distinct inflammatory state relative to PDGF-DD via NF-kappaB-dependent mechanisms. Physiological genomics. 2012; 44:417–429. DOI: 10.1152/physiolgenomics. 00160.2011 [PubMed: 22318995]

24. Libby P, Warner SJ, Friedman GB. Interleukin 1: a mitogen for human vascular smooth muscle cells that induces the release of growth-inhibitory prostanoids. J Clin Invest. 1988; 81:487–498. DOI: 10.1172/JCI113346 [PubMed: 3276731]

25. Loppnow H, Libby P. Proliferating or interleukin 1-activated human vascular smooth muscle cells secrete copious interleukin 6. J Clin Invest. 1990; 85:731–738. DOI: 10.1172/JCI114498 [PubMed: 2312724]

26. Baylis RA, Gomez D, Owens GK. Shifting the Focus of Preclinical, Murine Atherosclerosis Studies From Prevention to Late-Stage Intervention. Circ Res. 2017; 120:775–777. DOI: 10.1161/CIRCRESAHA.116.310101 [PubMed: 28254801]

27. Gomez D, Shankman LS, Nguyen AT, Owens GK. Detection of histone modifications at specific gene loci in single cells in histological sections. Nature methods. 2013; 10:171–177. DOI: 10.1038/nmeth.2332 [PubMed: 23314172]

28. Mombaerts P, et al. RAG-1-deficient mice have no mature B and T lymphocytes. Cell. 1992; 68:869–877. [PubMed: 1547488]

29. Amento EP, Ehsani N, Palmer H, Libby P. Cytokines and growth factors positively and negatively regulate interstitial collagen gene expression in human vascular smooth muscle cells. Arterioscler Thromb. 1991; 11:1223–1230. [PubMed: 1911708]

30. Alexander MR, et al. Genetic inactivation of IL-1 signaling enhances atherosclerotic plaque instability and reduces outward vessel remodeling in advanced atherosclerosis in mice. J Clin Invest. 2012; 122:70–79. DOI: 10.1172/JCI43713 [PubMed: 22201681]

31. Tacke F, et al. Immature monocytes acquire antigens from other cells in the bone marrow and present them to T cells after maturing in the periphery. J Exp Med. 2006; 203:583–597. DOI: 10.1084/jem.20052119 [PubMed: 16492803]

32. Potteaux S, et al. Suppressed monocyte recruitment drives macrophage removal from atherosclerotic plaques of Apoe−/− mice during disease regression. J Clin Invest. 2011; 121:2025–2036. DOI: 10.1172/JCI43802 [PubMed: 21505265]

33. Haka AS, Potteaux S, Fraser H, Randolph GJ, Maxfield FR. Quantitative analysis of monocyte subpopulations in murine atherosclerotic plaques by multiphoton microscopy. PLoS One. 2012; 7:e44823. [PubMed: 23024767]

34. Abdulaal WH, et al. Characterization of a conditional interleukin-1 receptor 1 mouse mutant using the Cre/LoxP system. Eur J Immunol. 2016; 46:912–918. DOI: 10.1002/eji.201546075 [PubMed: 26692072]

35. Clausen BE, Burkhardt C, Reith W, Renkawitz R, Forster I. Conditional gene targeting in macrophages and granulocytes using LysMcre mice. Transgenic Res. 1999; 8:265–277. [PubMed: 10621974]

36. Vadiveloo PK, Stanton HR, Cochran FW, Hamilton JA. Interleukin-4 inhibits human smooth muscle cell proliferation. Artery. 1994; 21:161–181. [PubMed: 7794123]

37. Hawker KM, Johnson PR, Hughes JM, Black JL. Interleukin-4 inhibits mitogen-induced proliferation of human airway smooth muscle cells in culture. Am J Physiol. 1998; 275:L469–477. [PubMed: 9728041]

38. Jenkins SJ, et al. Local macrophage proliferation, rather than recruitment from the blood, is a signature of TH2 inflammation. Science. 2011; 332:1284–1288. DOI: 10.1126/science.1204351 [PubMed: 21566158]

39. Jenkins SJ, et al. IL-4 directly signals tissue-resident macrophages to proliferate beyond homeostatic levels controlled by CSF-1. J Exp Med. 2013; 210:2477–2491. DOI: 10.1084/jem.20121999 [PubMed: 24101381]

40. Sica A, Mantovani A. Macrophage plasticity and polarization: in vivo veritas. J Clin Invest. 2012; 122:787–795. DOI: 10.1172/JCI59643 [PubMed: 22378047]

41. Zhao XN, Li YN, Wang YT. Interleukin-4 regulates macrophage polarization via the MAPK signaling pathway to protect against atherosclerosis. Genet Mol Res. 2016; 15

42. Tabas I. Macrophage death and defective inflammation resolution in atherosclerosis. Nat Rev Immunol. 2010; 10:36–46. DOI: 10.1038/nri2675 [PubMed: 19960040]

43. Cai B, et al. MerTK cleavage limits proresolving mediator biosynthesis and exacerbates tissue inflammation. Proc Natl Acad Sci U S A. 2016; 113:6526–6531. DOI: 10.1073/pnas.1524292113 [PubMed: 27199481]

44. van Gils JM, et al. The neuroimmune guidance cue netrin-1 promotes atherosclerosis by inhibiting the emigration of macrophages from plaques. Nat Immunol. 2012; 13:136–143. DOI: 10.1038/ni.2205 [PubMed: 22231519]

45. Wanschel A, et al. Neuroimmune guidance cue Semaphorin 3E is expressed in atherosclerotic plaques and regulates macrophage retention. Arterioscler Thromb Vasc Biol. 2013; 33:886–893. DOI: 10.1161/ATVBAHA.112.300941 [PubMed: 23430613]

46. Robbins CS, et al. Local proliferation dominates lesional macrophage accumulation in atherosclerosis. Nat Med. 2013; 19:1166–1172. DOI: 10.1038/nm.3258 [PubMed: 23933982]

47. Duewell P, et al. NLRP3 inflammasomes are required for atherogenesis and activated by cholesterol crystals. Nature. 2010; 464:1357–1361. DOI: 10.1038/nature08938 [PubMed: 20428172]

48. Baylis RA, Gomez D, Mallat Z, Pasterkamp G, Owens GK. The CANTOS Trial: One Important Step for Clinical Cardiology but a Giant Leap for Vascular Biology. Arterioscler Thromb Vasc Biol. 2017; 37:e174–e177. DOI: 10.1161/ATVBAHA.117.310097 [PubMed: 28970294]

49. Harrington RA. Targeting Inflammation in Coronary Artery Disease. N Engl J Med. 2017

50. Ibanez B, Fuster V. CANTOS: A Gigantic Proof-of-Concept Trial. Circ Res. 2017; 121:1320–1322. DOI: 10.1161/CIRCRESAHA.117.312200 [PubMed: 29217712]

51. Nov O, et al. Interleukin-1beta regulates fat-liver crosstalk in obesity by auto-paracrine modulation of adipose tissue inflammation and expandability. PLoS One. 2013; 8:e53626. [PubMed: 23341960]

52. Howard C, et al. Safety and tolerability of canakinumab, an IL-1beta inhibitor, in type 2 diabetes mellitus patients: a pooled analysis of three randomised double-blind studies. Cardiovasc Diabetol. 2014; 13:94. [PubMed: 24884602]

53. Everett BM, et al. Anti-Inflammatory Therapy with Canakinumab for the Prevention and Management of Diabetes. J Am Coll Cardiol. 2018

54. Topol EJ. Failing the public health--rofecoxib, Merck, and the FDA. N Engl J Med. 2004; 351:1707–1709. DOI: 10.1056/NEJMp048286 [PubMed: 15470193]

55. Morton AC, et al. The effect of interleukin-1 receptor antagonist therapy on markers of inflammation in non-ST elevation acute coronary syndromes: the MRC-ILA Heart Study. Eur Heart J. 2015; 36:377–384. DOI: 10.1093/eurheartj/ehu272 [PubMed: 25079365]

56. Interleukin 1 Genetics C. Cardiometabolic effects of genetic upregulation of the interleukin 1 receptor antagonist: a Mendelian randomisation analysis. Lancet Diabetes Endocrinol. 2015; 3:243–253. DOI: 10.1016/S2213-8587(15)00034-0 [PubMed: 25726324]

57. Wirth A, et al. G12-G13-LARG-mediated signaling in vascular smooth muscle is required for salt-induced hypertension. Nat Med. 2008; 14:64–68. DOI: 10.1038/nm1666 [PubMed: 18084302]

58. Dobin A, et al. STAR: ultrafast universal RNA-seq aligner. Bioinformatics. 2013; 29:15–21. DOI: 10.1093/bioinformatics/bts635 [PubMed: 23104886]

59. Liao Y, Smyth GK, Shi W. featureCounts: an efficient general purpose program for assigning sequence reads to genomic features. Bioinformatics. 2014; 30:923–930. DOI: 10.1093/bioinformatics/btt656 [PubMed: 24227677]

60. Love MI, Huber W, Anders S. Moderated estimation of fold change and dispersion for RNA-seq data with DESeq2. Genome Biol. 2014; 15:550. [PubMed: 25516281]

61. Luo W, Friedman MS, Shedden K, Hankenson KD, Woolf PJ. GAGE: generally applicable gene set enrichment for pathway analysis. BMC Bioinformatics. 2009; 10:161. [PubMed: 19473525]
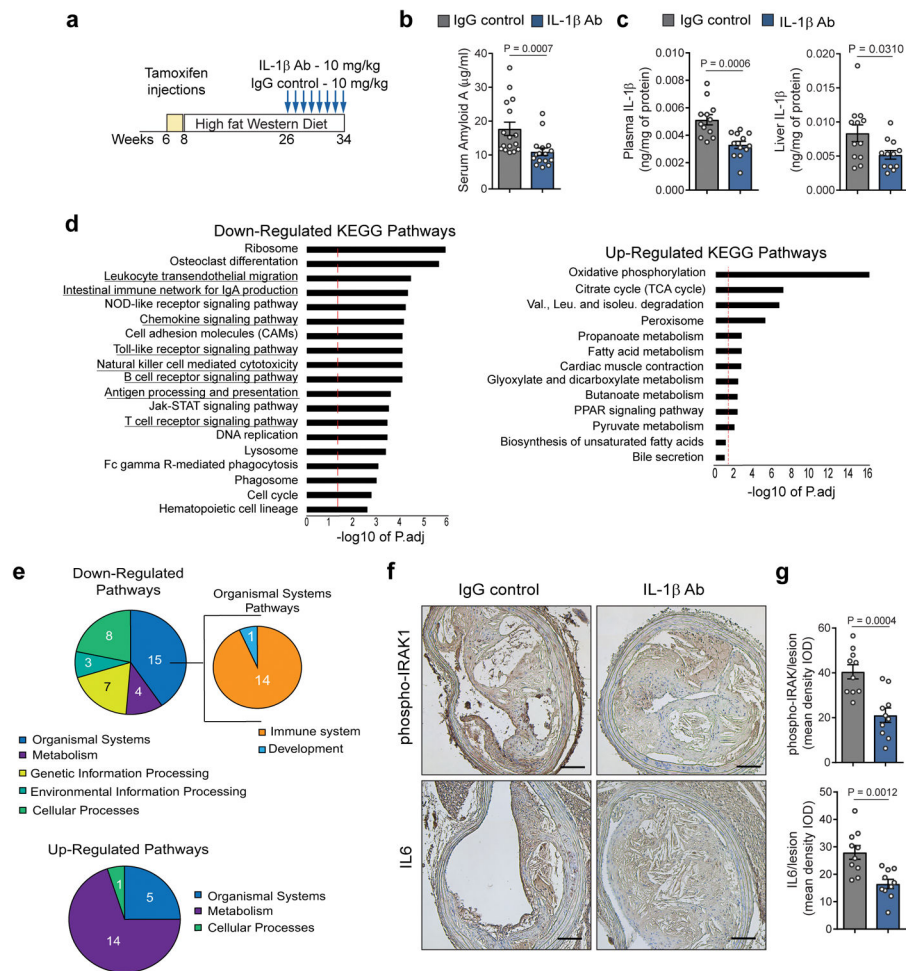
Figure 1. IL-1β antibody treatment results in systemic and local downregulation of IL-1 signaling and pro-inflammatory pathways

a – Schematic of intervention studies in which $Apoe^{-/-}$ $Myh11$ ER^{T2} Cre YFP mice fed a WD for 18 weeks were injected weekly with the IL-1β antibody or an isotype-matched IgG control antibody at a concentration of 10mg/kg for 8 weeks. (**b,c**) Assessment of systemic inflammation by quantification of plasma Serum Amyloid A (n=16 biologically independent animals per group) (**b**) and IL-1β in plasma (**c**, left) and liver (**c,** right) (n=12 biologically independent animals per group). Data were analyzed with a two-tailed non-parametric Mann-Whitney U-test (**b**) or a two-tailed unpaired t-test (**c**) (mean ± SEM). **d** – Results of RNA-seq analyses on tissue extracts from the BCA of IL-1β antibody and IgG control treated mice (n=4 biologically independent animals per group). Pathway-enrichment charts display pathways that were downregulated or upregulated in IL-1β antibody treated mice as compared to IgG control treated mice. The red lines indicate results that were significant with an adjusted P value of P_{adj} 0.05. Enrichment is shown as the $-\log_{10}$ of P_{adj} values. Underlined pathways are related to immunity and inflammation. **e** – Pie charts show functional annotation analyses of pathways downregulated (upper pie charts) or upregulated (bottom pie chart) in BCA extracts of IL-1β antibody treated mice as compared to IgG control treated mice as determined by RNAseq analysis. **f** – Representative images of

phospho-IRAK and IL-6 immunostaining in BCA sections of IgG control and IL-1β antibody treated mice. Scale bar, 100 μm. **g** – Quantification of phospho-IRAK and IL6 staining shown in **f** by integrated optical densitometry analysis (n=10 biologically independent animals per group). Two-tailed unpaired t-test (mean ± SEM).
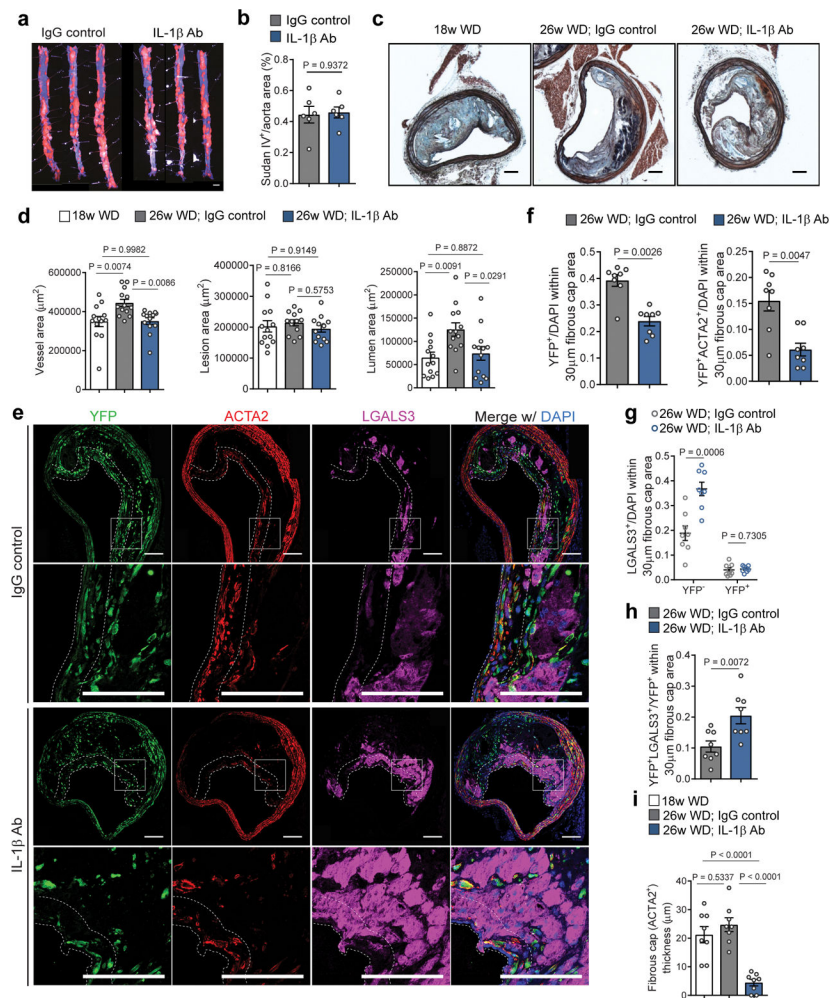
Figure 2. IL-1β inhibition induces multiple detrimental changes in the pathogenesis of late stage atherosclerotic lesions, including loss of an SMC-rich fibrous cap and inhibition of beneficial outward remodeling

a – Sudan IV staining of aortic plaque burden in IgG control and IL-1β antibody treated mice. Scale bar, 1mm. **b** – Quantification of Sudan IV positive area (n=6 biologically independent animals per group). Two-tailed unpaired *t*-test (mean ± SEM). **c** - Representative images of Movat stained BCA cross-sections obtained from 18 week WD fed, 26 week WD fed IgG control treated, and 26 week WD fed IL-1β antibody treated *Apoe* $^{-/-}$ *Myh11* ER^{T2} Cre YFP mice. Scale bar, 100 μm. **d** – Quantification of vessel, lesion and lumen areas of BCA cross-sections from cohorts of animals shown in **b** (n=13 biologically independent animals per group). One-Way Anova (mean ± SEM). **e** – Representative micrographs showing differences in the distribution of YFP+, LGALS3+, and ACTA2+ cells in the fibrous cap area of lesions in mice treated with the IL-1β antibody and the IgG control. The dashed lines delineates the 30μm fibrous cap area. The box indicates the region magnified in the lower panels. Scale bar, 100 μm. **f** – Quantification of the number of YFP+ and YFP+ACTA2+ cells normalized to the total number of cells within the fibrous cap area (n=8 biologically independent animals per group). Two-tailed non parametric Mann Whitney test (mean ± SEM). **g** – Quantification of the number of YFP−LGALS3+ and YFP

$^+$LGALS3$^+$ cells normalized to the total number of cells within the fibrous cap area (n=8 biologically independent animals per group). Two-tailed unpaired t-test (mean ± SEM). **h** – Proportion of YFP$^+$LGALS3$^+$ cells normalized to the SMC YFP$^+$ cell population within the fibrous cap (n=8 biologically independent animals per group). Two-tailed unpaired t-test (mean ± SEM). **i** – Fibrous cap thickness (μm) as determined by the average thickness of ACTA2+ cells from the endothelial layer (n=8 biologically independent animals per group). One way ANOVA (mean ± SEM).
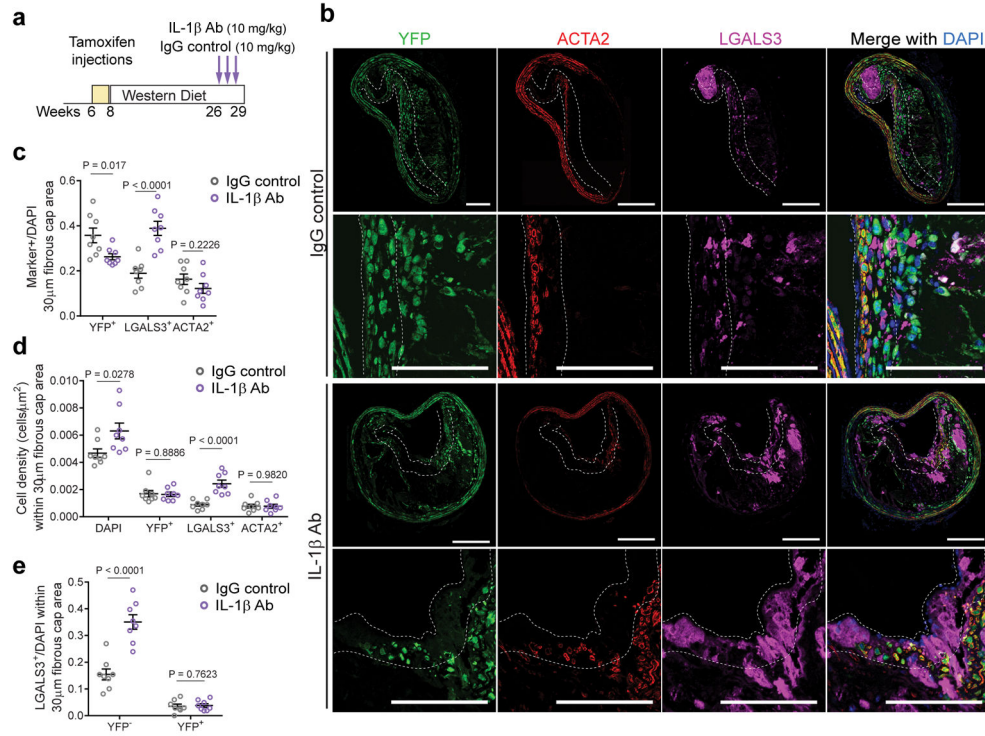
Figure 3. A three-week course of IL-1β antibody treatment results in an increased number of macrophages within the fibrous cap

a – Schematic of short-term treatment of *Apoe*^{−/−} *Myh11* ER[T2] Cre YFP fed a WD for 18 weeks with weekly injections with IL-1β or IgG control antibodies at a concentration of 10 mg/kg for 3 weeks (n=8 biologically independent animals per group). **b** – Representative micrographs showing differences in the distribution of YFP[+], LGALS3^{+} and ACTA2^{+} cells between IgG control and IL-1β antibody treated mice following 3 weeks of treatment. The dashed line delineates the 30μm fibrous cap area. Scale bar, 100 μm. **c** – Proportion of YFP[+], LGALS3^{+} and ACTA2^{+} cells normalized to the total number of cells within the fibrous cap area. **d** – The number of cells normalized to the area of the fibrous cap (μm[2]). **e** – Quantification of the number of YFP[−]LGALS3^{+} cells versus the number of YFP[+]LGALS3^{−} cells within the fibrous cap. Data were analyzed by two-tailed unpaired *t*-tests (mean ± SEM).
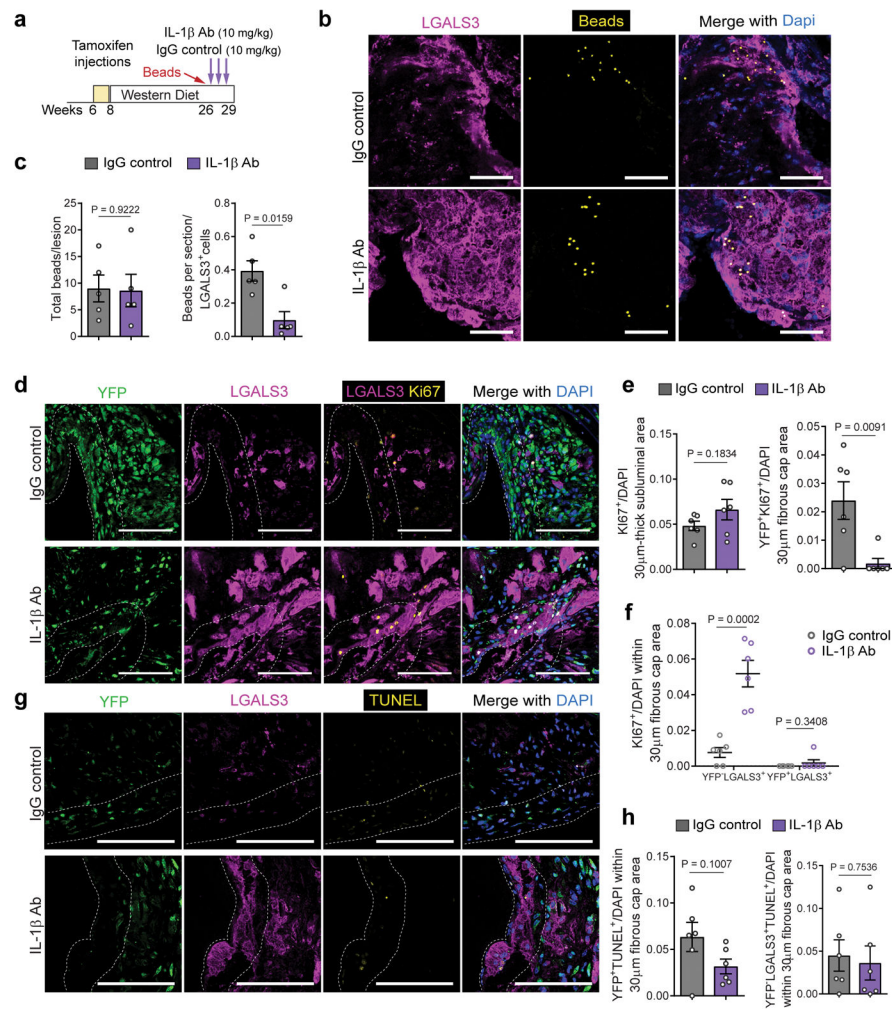
Figure 4. IL-1β inhibition for three-weeks results in increased proliferation of local macrophages but no change in monocyte trafficking or apoptosis

a – Schematic representing the experimental design of bead uptake assays performed in *Apoe*$^{-/-}$ *Myh11* ER^{T2} Cre YFP mice treated with IL-1β antibody or IgG control. **b** – Representative micrographs of bead uptake within BCA lesions. The lesions were stained for LGALS3$^+$ and Cy3-labeled beads were visualized. Scale bar, 100 μm. **c** – Quantification of bead uptake showing the total number of beads per section (left) and the number of beads normalized to the number of LGALS3$^+$ cells (right) (n=5 biologically independent animals per group). Two-tailed unpaired t-test (Total bead) and two-tailed non-parametric Mann-Whitney (Beads/LGALS3$^+$) (mean ± SEM). **d** – Representative micrographs for assessment of cell proliferation. BCA sections of IL-1β antibody treated and control mice were stained for YFP, LGALS3 and KI67. Scale bar, 100 μm. (**e & f**) – Quantification of the number of KI67$^+$ cells and KI67$^+$ subpopulations (Ki67$^+$YFP$^+$ and Ki67$^+$LGALS3$^+$; n=6 animals per group). Data were analyzed using two-tailed unpaired *t*-test (mean ± SEM). **g** – Representative micrographs for assessment of cell apoptosis. BCA sections of IL-1β antibody treated and control mice were stained for YFP, LGALS3 and TUNEL. Scale bar, 100 μm. **h** – Quantification of the number of TUNEL$^+$ subpopulations (YFP$^+$ and YFP

⁻LGALS3⁺; n=6 animals per group). Data were analyzed using two-tailed unpaired t-test. Data are presented as mean ± SEM.
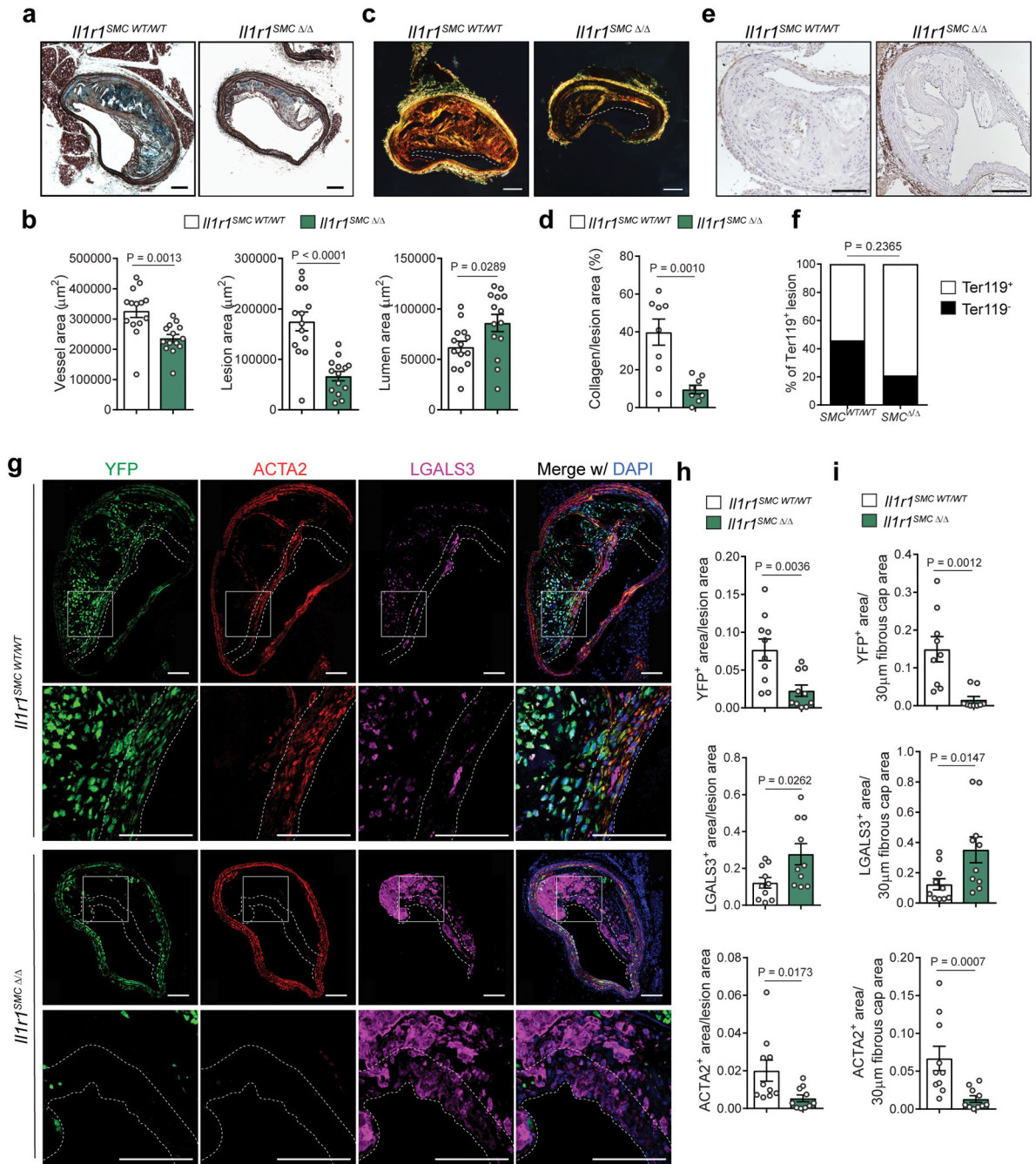
Figure 5. IL-1 signaling within SMCs is required for SMC investment into the lesion and the fibrous cap

a – Movat staining of BCA sections from $Il1r1^{SMC\ WT/WT}$ and $Il1r1^{SMC\ \Delta/\Delta}$ littermates fed a WD for 18 weeks. **b** – Morphometric analysis of the vessel, lesion, and lumen areas of $Il1r1^{SMC\ WT/WT}$ and $Il1r1^{SMC\ \Delta/\Delta}$ BCA cross-sections (n = 14 biologically independent animals per group). **c** – Representative images of Picrosirius Red staining, as visualized by polarized light. **d** – Quantification of collagen content as a percentage of lesion area (n = 8 animals per group). **e** – Representative images of Ter119 staining, used to detect intraplaque

hemorrhage. **f** – Distribution of intraplaque hemorrhage positive and negative lesions in *Il1r1^{SMC WT/WT}* and *Il1r1^{SMC ∆/∆}* mice. **g** – Immunofluorescent staining of BCA sections from *Il1r1^{SMC WT/WT}* and *Il1r1^{SMC ∆/∆}* mice for YFP, ACTA2 and LGALS3. High magnification images of the fibrous cap are shown of the region indicated by a box. **h–i** – Quantification of pixels in the YFP⁺, ACTA2⁺, and LGALS3⁺ areas normalized to the lesion area (**h**) and to the 30 μm fibrous cap area (**i**) (n = 10 biologically independent animals per group). Data were analyzed with two-tailed unpaired *t*-tests (**b,d**), a two-tailed exact Fisher test (**f**), or two-tailed non-parametric Mann-Whitney *U*-tests (**h,i**) and presented as the mean ± SEM. Scale bar, 100 μm (**a,c,e,g**).
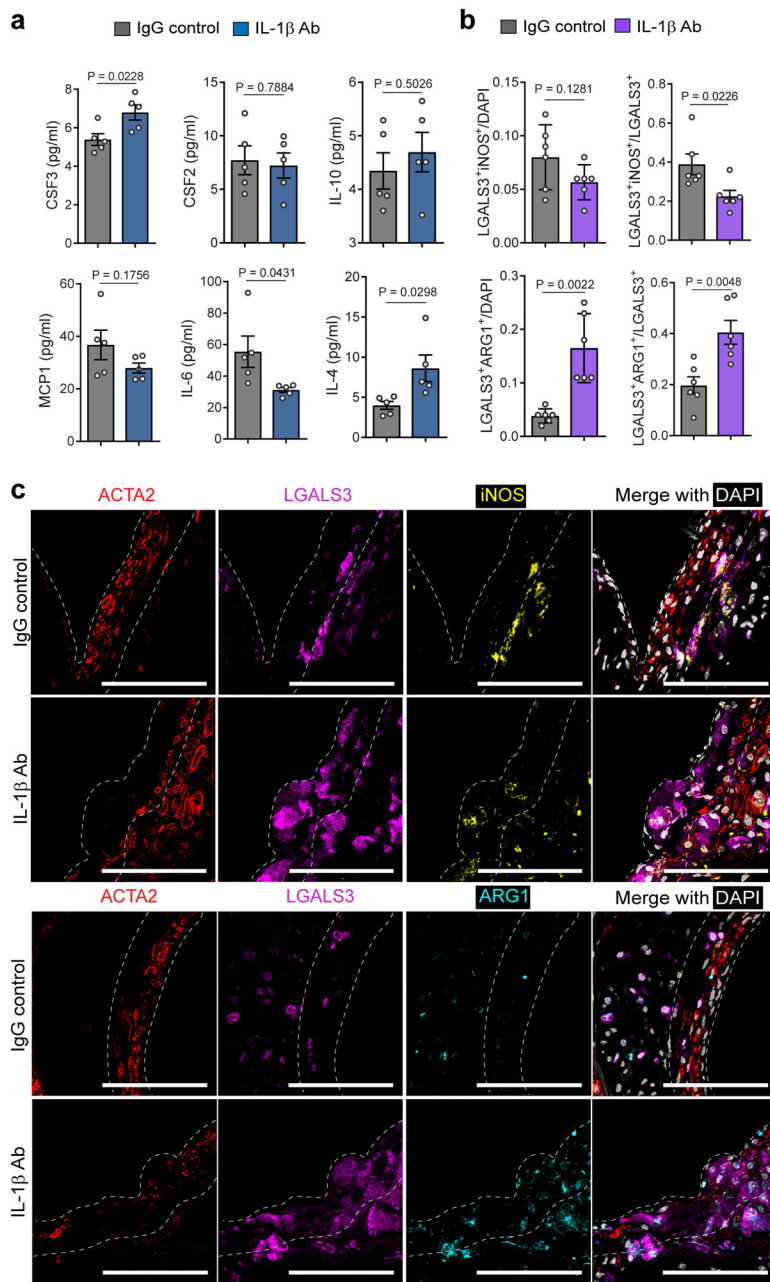
Figure 6. IL-1β inhibition is associated with polarization of fibrous cap macrophages to an M2 phenotype

a –Abundance of the indicated proteins (monocyte and macrophage colony stimulating factors (CSF2 and CSF3), monocyte chemoattractant CCL2, pro-inflammatory cytokine IL-6 and anti-inflammatory cytokines IL-10 and IL-4) in protein extracts from the BCA of mice treated with IL-1β antibody or control IgG antibody for 8 weeks, as assessed by a cytokine and chemokine array (n=5 animals per group). **b** – Quantification of the number of LGALS3+iNOS+ and LGALS3+ARG1+ cells normalized to the total number of cells or the total number of LGALS3+ cells in BCA lesions of mice treated for 3 weeks with IL-1β antibody or IgG control (n=6 animals per group). **c** – Representative micrographs of

immunostaining for ACTA2, LGALS3, the M1 marker iNOS (upper panels) or the M2 marker Arg1 (lower panels). Scale bar, 100 μm. Data were analyzed using two-tailed unpaired *t*-test and presented as the mean ± SEM.